

CityLoc: 6DoF Pose Distributional Localization for Text Descriptions in Large-Scale Scenes with Gaussian Representation

Qi Ma¹ Runyi Yang² Bin Ren^{2,3,4} Nicu Sebe⁴ Ender Konukoglu¹ Luc Van Gool^{1,2} Danda Pani Paudel²

Abstract

Localizing textual descriptions within large-scale 3D scenes presents inherent ambiguities, such as identifying all traffic lights in a city. Addressing this, we introduce a method to generate distributions of camera poses conditioned on textual descriptions, facilitating robust reasoning for broadly defined concepts. Our approach employs a diffusion-based architecture to refine noisy 6DoF camera poses towards plausible locations, with conditional signals derived from pre-trained text encoders. Integration with the pretrained Vision-Language Model, CLIP, establishes a strong linkage between text descriptions and pose distributions. Enhancement of localization accuracy is achieved by rendering candidate poses using 3D Gaussian splatting, which corrects misaligned samples through visual reasoning. We validate our method's superiority by comparing it against standard distribution estimation methods across five large-scale datasets, demonstrating consistent outperformance. Code, datasets and more information will be publicly available at our project page.

1. Introduction

With the emergence of multi-modal understanding at scale, the integration of text and visual inputs has become increasingly intertwined. Although these modalities are complementary, they are not always available jointly. Therefore, methods such as CLIP (Radford et al., 2021), DALLE (Ramesh et al., 2021), LLaVA (Liu et al., 2023c), and others (Li et al., 2024; Lin et al., 2024; Wang et al., 2023c; Bai et al., 2023; Zhu et al., 2023b; Chen et al., 2023; Peng et al., 2023), have been developed to bridge the gap between these modalities across various tasks. In this work, we aim to estimate pose distributions within a city-scale visual

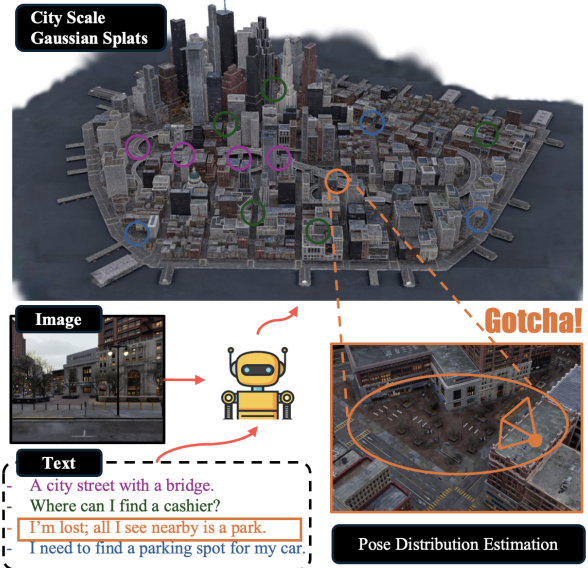


Figure 1. CityLoc: Given an ambiguous text description, our method accurately estimates the camera pose distribution across a large-scale urban environment, pinpointing probable locations like parking spots. Using Vision-Language Models (VLMs), our approach also incorporates image inputs for more precise, context-aware pose localization.

environment, leveraging textual descriptions, where the 3D contextual environment is already known. Our motivation for pursuing this research is twofold: (i) To decode visual locations from human language descriptions, facilitating natural human-robot interactions; (ii) To enable large language models (LLMs) to navigate and interpret visual scenes using language tokens. Our goal is to achieve text-based 6 degrees of freedom (6DoF) localization in expansive scenes where conventional feed-forward processing is impractical.

Text-based 6DoF localization in large 3D scenes, driven by our motivations, is inherently ambiguous. For instance, consider the scenario described by *"building next to the street near a traffic light and zebra crossings"* which can apply to numerous locations. We aim to achieve distributional localization that accounts for all potential instances that fit a given textual description, *i.e.*, we intend to generate a distribution of camera poses conditioned on the text description.

¹Computer Vision Lab, ETH Zurich ²INSAIT, Sofia University

³University of Pisa ⁴University of Trento. Correspondence to: Bin Ren <bin.ren@insait.ai>.

To achieve this, we construct a dataset of pose-text pairs using Large Multimodal Model. We then propose a diffusion-based conditional distribution learning technique to iteratively refine noisy initial poses by conditioning on mixed visual-text features. Our approach stands in contrast to existing methods cited in (Kolmet et al., 2022; Xia et al., 2024), which seek the most probable pose and depend on highly detailed textual descriptions.

For visual representation, we use multiple large-scale 3D Gaussian scenes as shown in Fig. 2, built in-house using a recent hierarchical 3D Gaussian method (Kerbl et al., 2024). This allows us to rasterize 2D images from specified 6DoF poses, facilitating visual reasoning based on the outputs of diffusion models. While the diffusion process could be conditioned on these rasterized images to enhance localization precision (Wang et al., 2023b), for efficiency in city-scale tasks, we avoid direct conditioning. Instead, we refine pose candidates through a two-step approach: (i) Initial filtration of pose candidates to remove unlikely poses, and (ii) Subsequent refinement of poses by comparing the input text with descriptions from the rasterized 2D images. Our method’s effectiveness is demonstrated in handling both single-modality scenarios with only text and multi-modal settings that integrate images and text.

Our method significantly differs from existing works like PoseDiffusion (Wang et al., 2023b), Text2Pose (Kolmet et al., 2022), Text2Loc (Xia et al., 2024), and RET (Wang et al., 2023a). PoseDiffusion, designed for central objects with deterministic poses, struggles with text-driven ambiguity and scale, relying on multi-view adjustments that falter in large-scale settings. In contrast, Text2Pose, Text2Loc, and RET depend on precise textual descriptions for 2D localization, lacking visual reasoning and proving inefficient in our experiments due to diverse scenes, sparse text, and the challenges of estimating 6DoF poses.

We deploy our method across 5 diverse large-scale scenes, covering over 10 square kilometers and featuring various viewpoints from street-level to aerial. These scenes include both urban and suburban environments in real and simulated formats. To ensure varied text descriptions during training, we utilize Llava (Liu et al., 2023c). During testing, we evaluate performance across varying levels of description granularity, incorporating both textual and visual inputs. Our results show that more detailed descriptions significantly enhance localization accuracy, affirming our method’s effectiveness in varied settings.

The contributions of this work are:

1. Experimental Setup and Benchmarking: We established a robust experimental framework to assess city-scale, text-based 6DoF pose distribution estimation, incorporating corresponding large scale Gaussian splats



Figure 2. We present qualitative results of our large-scale Gaussian splats, including the number of images and the trained Gaussian memory size for each scene.

as 3D representation.

2. Novel Approach for Text-Based 6DoF Localization: We present a novel diffusion-based approach that integrates mixup training with multimodal image-text features using CLIP. This method effectively bridges the gap between textual descriptions and accurate spatial localization, achieving robust performance in large-scale urban environments.
3. Pose Refinement Technique: We employ Gaussian splatting rendering to enhance the pose accuracy, discarding mismatches and optimizing alignment by leveraging cosine similarity with text features. This ensures the refined pose corresponds precisely to the most relevant location based on the provided text description.
4. State-of-the-Art Results: Our approach delivers superior performance, surpassing baseline methods in both pose estimation accuracy and distribution modeling.

2. Related Work

Diffusion Model. Diffusion models (Sohl-Dickstein et al., 2015; Ho et al., 2020; Dhariwal & Nichol, 2021), inspired by non-equilibrium thermodynamics, approximate complex data distributions by reversing a noise addition process through a series of diffusion steps. Originally developed for generative tasks, these models have demonstrated impressive results in image (Ho et al., 2020; Song et al., 2020; Dhariwal & Nichol, 2021; Wang et al., 2022), video (Singer et al., 2022; Ho et al., 2022), and 3D point cloud generation (Lyu et al., 2021; Zhao et al., 2024; Liu et al., 2023a; Ren et al., 2024), as well as in natural language (Austin et al., 2021; Li et al., 2022) and audio generation (Popov et al., 2021). More recently, diffusion models have been adapted for discriminative tasks, including image segmentation (Amit et al., 2021; Brempong et al., 2022) and visual grounding. However, there has been little exploration of applying diffusion models to camera localization tasks. In this work, we leverage the iterative nature of diffusion to re-

fine probabilistic spatial representations for accurate camera pose estimation. By modeling spatial correlations through a Gaussian representation, we progressively refine the 6 DoF camera pose, achieving high precision and robustness in large-scale scenes, thus showcasing the flexibility of diffusion models in localization and scene understanding.

Multi-Modal Large Language Models. To extend the advancements of language models (Brown et al., 2020; Touvron et al., 2023; Chowdhery et al., 2023; Le Scao et al., 2023; Hoffmann et al., 2022) across modalities, Multi-Modal Large Language Models (MLLMs) integrate language and vision (Yin et al., 2023; Liu et al., 2024b; Zhu et al., 2023a; Alayrac et al., 2022; Zheng et al., 2024). These models excel in tasks requiring an understanding of both text and images, which is relevant for camera localization in large-scale scenes. Flamingo (Alayrac et al., 2022) was among the first to align image-text pairs using gated cross-attention blocks, highlighting the importance of multi-modal integration. In 6 DoF camera localization, MLLMs enhance the interpretation of complex urban environments by integrating semantic information from both modalities. End-to-end MLLMs often fine-tune intermediate networks (Lai et al., 2024; Zhang et al., 2023) or sampler modules (You et al., 2023) to map visual features into the language space, improving scene representations for localization tasks. Models like BLIP-2 (Li et al., 2023b), MiniGPT-4 (Zhu et al., 2023a), and LLava (Liu et al., 2024b) bridge modality gaps using querying transformers and two-stage training processes, demonstrating the effectiveness of combining visual and textual data to enhance localization accuracy. Other notable models such as Otter (Li et al., 2023a), mPLUG-Owl (Ye et al., 2023), and InstructBLIP (Dai et al., 2024) offer architectural inspirations. Drawing from these MLLMs, our method utilizes Gaussian representations (Kerbl et al., 2023) to improve 6 DoF camera localization in large-scale scenes, enhancing both accuracy and computational efficiency.

Large-scale 3D Representation and Localization. Recent advancements in view synthesis, such as NeRFs (Mildenhall et al., 2021; Barron et al., 2021; Müller et al., 2022; Barron et al., 2022; Wu et al., 2023) and 3DGS (Kerbl et al., 2023; 2024; Liu et al., 2024c; Ma et al., 2025; Yang et al., 2024; Lou et al., 2024), have revolutionized 3D scene representation by utilizing differentiable rendering and optimization. To address the problem of large scenes, several methods have divided scenes into blocks or using multi-level decompositions, such as Mega-NeRF (Turki et al., 2022), Block-NeRF (Tancik et al., 2022), CityGaussian (Liu et al., 2024c), and hierarchical 3DGS (Kerbl et al., 2024).

Localization and mapping are closely linked, with high-quality 3D reconstructions aiding visual localization. Methods like PoseNet (Kendall et al., 2015) predict camera poses but struggle in large environments. iNeRF (Yen-Chen et al., 2021) and iGS (Sun et al., 2023) invert NeRFs and 3DGS for

6DoF pose estimation. Text-based methods like Text2Pos (Kolmet et al., 2022) and Text2Loc (Xia et al., 2024) generate poses from descriptions, but can suffer from ambiguity. In contrast, our method learns a distribution of poses from text and refines them using a 3DGS map, marking the first work to bridge text descriptions with pose distributions and use Gaussian representations for large-scale pose refinement.

Algorithm 1 Mixup Training Algorithm

Require:

Inputs:

- Image embedding \mathcal{T}_f and text embedding \mathcal{T}_t
- Random pose P_{rand} and ground truth pose P_{gt}
- Swap ratio $\beta \in [0, 1]$ (hyperparameter)
- Denoiser \mathcal{F}_θ

Ensure: Estimate the pose distribution $p(P \mid \mathcal{T})$

- 1: **for** epoch = 1 to N **do**
- 2: **for** each batch $(\mathcal{T}_f, \mathcal{T}_t, P_{\text{gt}}) \in \mathcal{D}$ **do**
- 3: Sample a timestamp $t \sim \text{Uniform}(\{1, \dots, T\})$
- 4: Random Sample embeddings:
- 5: $\mathcal{T}_{\text{mix}} \leftarrow \begin{cases} \mathcal{T}_t & \text{with swap ratio } \beta, \\ \mathcal{T}_f & \text{with swap ratio } 1 - \beta. \end{cases}$
- 6: Sample noise and predict noise
- 7: Predict pose: $P_{\text{pred}} \leftarrow h_{\text{DDPM}}(\mathcal{T}_{\text{mix}}, P_{\text{rand}})$
- 8: Compute loss: $\mathcal{L} \leftarrow \|P_{\text{pred}} - P_{\text{gt}}\|^2$
- 9: Update model: $\mathcal{F}_\theta \leftarrow \arg \min_h \mathbb{E}[\mathcal{L}]$
- 10: **end for**
- 11: **end for**
- 12: **return** \mathcal{F}_θ

3. Proposed Method

The CityLoc pipeline, illustrated in Fig. 3, integrates the Vision Language Model (VLM) as a condition to achieve multi-modal localization. It further refines pose distribution estimation by aligning cross-modal features, minimizing the discrepancy between the rendered image feature embeddings and the input text feature embeddings. In the following sections, we will discuss each component of the pipeline in detail.

Problem Setting. We address 6-DoF pose distribution estimation by combining text and image features in a multi-modal framework. This approach integrates scene descriptions (e.g., textual or visual cues) to enhance pose distribution estimation. First, we extract CLIP features for both text and image data, denoted as $\mathcal{T}_t, \mathcal{T}_f \in \mathbb{R}^d$. Formally, given an input text feature \mathcal{T}_t^i or image feature \mathcal{T}_f^i , our goal is to estimate the pose distribution $p(P \mid \mathcal{T}^i)$ that aligns with the corresponding feature description \mathcal{T}^i . This is achieved



Figure 3. Overview of CityLoc. In the training process, where images and multi-level of granularity text input are first converted to CLIP features. A mix algorithm combines these features to train a pose diffusion model, mapping them to a 6DoF camera pose distribution. In the inference phase, where the pose diffusion model outputs camera poses for any given text input. A pretrained Gaussian representation is used to refine the poses, aligning the input text features with the rendered image features.

by sampling M discrete pose candidates $\{P^{i,j}\}_{j=1}^M$, where each $P^{i,j} \in \mathbb{SE}(3)$ represents a likely pose associated with the given text or image input.

Algorithm 2 Gaussian Refinement Algorithm

Require:

Inputs:

- Initial coarse pose P_{coarse} , Ground Truth pose P_{gt}
- Input text embedding T_t from CLIP Encoder f_{CLIP}
- City-scale Gaussian model \mathcal{G}
- Hyperparameters: learning rate η , iterations N

Ensure: Refined camera pose P_{refined} , success flag success

```

1: Initialize  $P_{\text{pred}} \leftarrow P_{\text{coarse}}$ , optimizer: Adam( $P_{\text{pred}}, \eta$ )
2: Render  $\hat{I} \leftarrow \mathcal{G}(P_{\text{pred}})$ 
3: Compute  $\hat{T}_f \leftarrow f_{\text{CLIP, img}}(\hat{I})$ 
4:  $\mathcal{L}_{\text{init}} \leftarrow \frac{\hat{T}_f^\top \cdot T_t}{\|\hat{T}_f\|_2 \cdot \|T_t\|_2}$ 
5: if  $\mathcal{L}_{\text{init}} < \tau_1$  then
6:   return  $P_{\text{pred}}$ , False            $\triangleright$  Reject poor initial pose
7: end if
8: for  $k = 1$  to  $N$  do
9:   Render  $\hat{I} \leftarrow \mathcal{G}(P_{\text{pred}})$ 
10:  Compute  $\hat{T}_f \leftarrow f_{\text{CLIP, img}}(\hat{I})$ 
11:   $\mathcal{L}_{\text{clip}} \leftarrow \frac{\hat{T}_f^\top \cdot T_t}{\|\hat{T}_f\|_2 \cdot \|T_t\|_2}$ 
12:  Backpropagate  $-\mathcal{L}_{\text{clip}}$  to update  $P_{\text{pred}}$ 
13: end for
14: if  $\mathcal{L}_{\text{clip}} < \tau_2$  then
15:   return  $P_{\text{pred}}$ , False            $\triangleright$  Reject refinement
16: end if
17: return  $P_{\text{pred}}$ , True

```

3.1. Diffusion-based pose estimation

CityLoc models the conditional probability distribution $p(P|\mathcal{T})$ of pose parameters P given features \mathcal{T} .

Using a diffusion-based model (Sohl-Dickstein et al., 2015; Wang et al., 2023b), we model $p(P|\mathcal{T})$ with a denoising process. Specifically, $p(P|\mathcal{T})$ is estimated by training a diffusion model \mathcal{F}_θ on a training set $\mathcal{S} = \{(P_j, \mathcal{T}_j)\}_{j=1}^M$ of $M \in \mathbb{N}$ locations with input textual and visual features \mathcal{T}_j and ground truth pose parameters P_{gt} . At inference, for a new set of text features \mathcal{T} , we sample $p(P|\mathcal{T})$ to estimate pose parameters P . The denoising process is conditioned on \mathcal{T} , i.e., $, p_\theta(P_{t-1} | P_t, \mathcal{T})$:

$$p_\theta(P_{t-1} | P_t, \mathcal{T}) = \mathcal{N}(P_{t-1}; \sqrt{\alpha_t} \mathcal{F}_\theta(P_t, t, \mathcal{T}), (1 - \alpha_t) \mathbb{I}). \quad (1)$$

Denoiser \mathcal{F}_θ . The denoiser \mathcal{F}_θ is implemented as a Transformer:

$$\mathcal{F}_\theta(P_t, t, \mathcal{T}) = \text{Trans} \left[\left(\text{cat}(P_t^i, t, \psi(T^i)) \right)_{i=1}^N \right] = \mu_{t-1}. \quad (2)$$

Here, the Transformer processes a sequence of noisy tuples P_t^i , time t , and embeddings $\psi(T^i) \in \mathbb{R}^{D_\psi}$ of text features T^i , outputting the corresponding denoised parameters $\mu_{t-1} = (\mu_{t-1}^i)_{i=1}^N$. Training \mathcal{F}_θ is supervised by the denoising loss:

$$\mathcal{L}_{\text{diff}} = E_{t \sim [1, T], P_t \sim q(P_t | P_0, \mathcal{T})} \|\mathcal{F}_\theta(P_t, t, \mathcal{T}) - P_0\|^2, \quad (3)$$

where the expectation aggregates over all diffusion steps t , the diffused samples $P_t \sim q(P_t | P_0, \mathcal{T})$, and a training set $\mathcal{S} = \{(P_{0,j}, \mathcal{T}_j)\}_{j=1}^M$ of scenes with features \mathcal{T}_j and poses $P_{0,j}$. Following DDPM sampling (Ho et al., 2020),

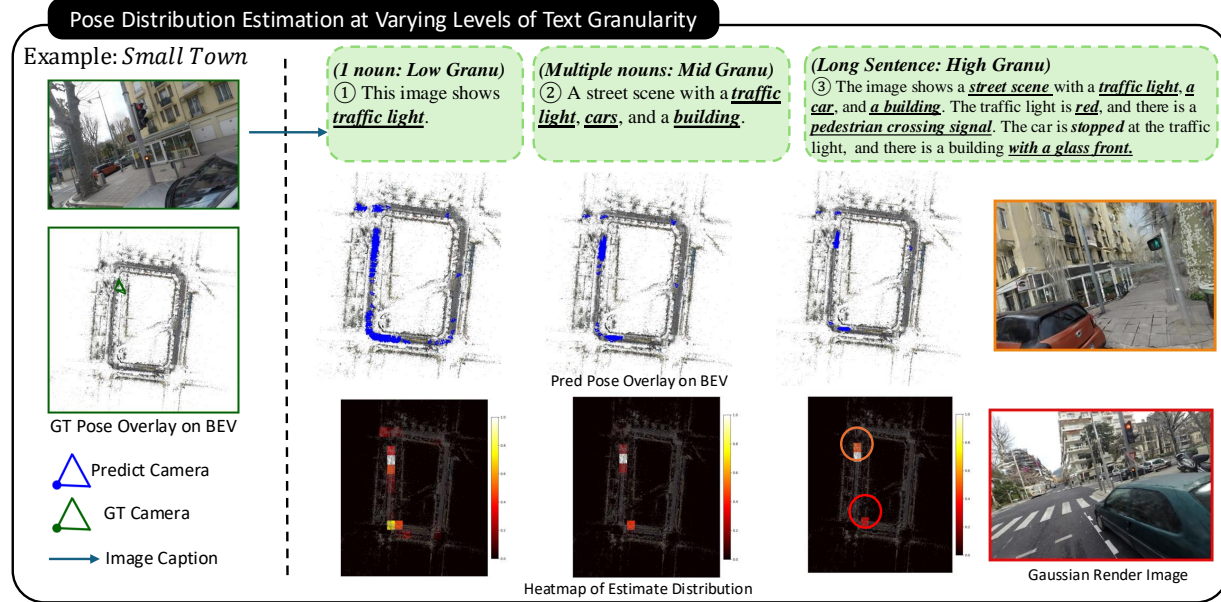


Figure 4. Qualitative results on the small town dataset: The enlarged green camera and its corresponding images represent those used to generate multiple text prompts with varying levels of granularity. We report the pose distribution conditioned on different levels of text details. The results clearly demonstrate that more informative text inputs lead to more precise location estimates. Additionally, cameras estimated in other locations provide meaningful insights. This is illustrated by selecting a pose within a high-density area for rendering as shown in red camera and orange camera, where both estimates reveal the presence of a traffic light. Zoom in for better visual results.

we initialize with random parameters $P_T \sim \mathcal{N}(\mathbf{0}, \mathbb{I})$ and, at each iteration $t \in (T, \dots, 0)$, sample the next step c_{t-1} as:

$$P_{t-1} \sim \mathcal{N}(P_{t-1}; \sqrt{\bar{\alpha}_{t-1}} \mathcal{F}_\theta(P_t, t, \mathcal{T}), (1 - \bar{\alpha}_{t-1}) \mathbb{I}). \quad (4)$$

Text-Prompt Generation. To construct the dataset with pose-text pairs, we extend image-pose pairs by generating captions using LLava-NEXT model (Liu et al., 2023c,b; 2024a) to process images at varying granularities. The text generation conditions on a question argument that specifies the desired level of detail in the captions, as outlined below:

- **Nouns:** Generates a list of up to ten nouns that capture the primary visual elements present in the image.
- **Template for Nouns Usage:** The extracted nouns are formatted as "A view of [nouns]" for input into the CLIP model, as seen in the upper right part of Fig. 3.
- **Long Sentence:** Produces a detailed caption composed of three concise sentences, providing a comprehensive description of the image.
- **Mid Sentence:** Delivers a balanced description in two sentences, offering an optimal trade-off between detail and conciseness.
- **Short Sentence:** Condenses the image content into a single succinct sentence, emphasizing the most prominent features.

Afterward, we calculate embedding cosine similarity of text and image, filtering out text descriptions not matching.

Multi-model Conditioning We propose the Mixup Training Algorithm (Alg. 1) to bridge the gap between input textual descriptions and predicted camera poses by introducing a novel embedding combination strategy during training. First, embeddings are generated for images and texts using a CLIP Image Encoder and a CLIP Text Encoder, respectively. These embeddings are then sampled using a hyper-parameter swap ratio for each data batch shown in step 4 of (Alg. 1). By minimizing the mean squared error between the predicted and ground truth poses, the model is optimized to embed multi-model information into the pose distribution estimation. This approach ensures a robust alignment between text, image and the pose and achieves accurate pose distribution estimation in large-scale, complex environments. By minimizing the mean squared error between the predicted and ground truth poses, the model is optimized to effectively integrate multi-modal information into the pose distribution estimation process. This optimization ensures strong generalization across diverse textual inputs by leveraging alignment between text and visual modalities through combined conditioning. As a result, the model achieves accurate and reliable pose likelihood prediction, even in large-scale, complex environments.

3.2. Text and Gaussian based Refinement

Unlike image-based refinement (Sun et al., 2023), which optimizes individual poses for a given image, our approach focuses on refining pose distributions using only text as input

User Study



Figure 5. An example question from the user study and its corresponding qualitative results. Ground-truth (GT) images appear on the left, while the rendered images are shown on the right. Quantitative results of user study please refer to Tab. 3.

to improve distribution estimation. As shown in Alg. 2, we begin with an initial coarse pose samples \hat{P}_{coarse} , derived through a diffusion process conditioned on text descriptions. This estimate serves as a probabilistic initialization for our pose configuration.

From this initial estimate, we render an image $\hat{I}_i = \mathcal{G}(\hat{P}_i)$ using rasterization from a trained Gaussian model \mathcal{G} .

We compute the cosine similarity between the CLIP embedding features of the rendered image and the CLIP embedding of the text input. If the similarity score is smaller than a threshold τ_1 , the sample is excluded from the distribution estimation. The negative of this similarity score is used as the loss function, which is backpropagated to refine the pose. Through this process, the coarse pose is iteratively updated to maximize the feature-level alignment with the text embedding. Finally, if the similarity score exceeds a second threshold τ_2 , the refined sample is accepted and saved.

4. Experiments

4.1. Experimental Settings

We evaluate the performance of CityLoc on a diverse set of datasets. First, we assess our method on the Small Town dataset (Kerbl et al., 2024), a large-scale collection comprising 5,822 images covering an area of over 40,000 m², with camera poses extracted using COLMAP (Schönberger & Frahm, 2016). Additionally, we test our approach on the UrbanScene3D dataset (Lin et al., 2022), which contains high-resolution drone imagery of expansive urban environments. The initial GPS-derived camera poses are refined

through a data preprocessing procedure based on MegaN-eRF (Turki et al., 2022). Finally, we evaluate CityLoc on the extensive MatrixCity dataset (Li et al., 2023c), which includes 67,000 aerial images and 452,000 street-level images spanning two city maps with a total area of 28 km².

Datasets					
Town	Residence	Sciart	Street	Aerial	
k = 15					
MCDrop	7.72	4.30	6.29	1.26	0.27
Ours	16.91	6.23	19.60	16.44	10.50
Ours Mixup	22.62	10.21	32.01	7.96	9.69
Ours Refined	26.37	12.42	34.69	15.11	13.21
k = 10					
MCDrop	8.69	6.10	4.46	1.98	0.25
Ours	15.21	14.01	28.32	29.86	19.90
Ours Mixup	35.33	20.26	43.61	12.76	18.18
Ours Refined	41.46	24.21	44.39	23.24	20.03
k = 5					
MCDrop	3.07	3.20	0.09	2.45	0.20
Ours	11.68	25.83	27.82	76.46	47.13
Ours Mixup	55.35	25.93	36.47	27.57	35.51
Ours Refined	57.21	28.85	39.92	35.21	39.22

Table 1. RDA Performance comparison across five datasets for different methods under three values of k explained in Fig. 6. We present three variants of our method: Ours (image only in training), Ours Mixup (image mixed with text prompt), and Ours Refined (Mixup with Gaussian splatting-based refinement). Best results per row are highlighted in red. Town, Street, Aerial are refer to Small Town, Matrix City Street and Matrix City Aerial respectively.

In our experimental setup, image description granularity

Datasets					
	Town	Residence	Sciart	Street	Aerial
Low Granularity					
Ours	2.73	1.09	1.18	1.75	2.12
Ours Mixup	5.96	10.67	7.97	1.89	2.72
High Granularity					
Ours	3.70	1.53	2.32	1.59	1.81
Ours Mixup	18.69	24.84	19.89	2.98	5.43
Max Granularity					
Ours	83.75	35.75	126.70	105.07	61.70
Ours Mixup	80.45	96.18	120.61	41.13	43.38

Table 2. *Granularity Experiments*. We compare **Ours** and **Ours Mixup** across five datasets under three granularity levels (Low, High, Max), and report the RDA value of different granularity of the methods accordingly. Town, Street, Aerial are refer to Small Town, Matrix City Street and Matrix City Aerial respectively.

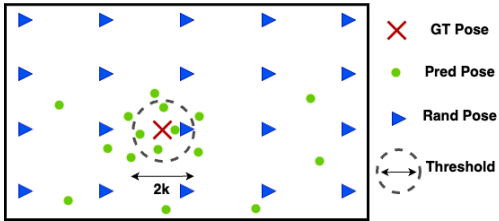


Figure 6. **Relative Distribution Accuracy (RDA)** measures the accuracy of the sample distribution within a specified region, defined by a distance k . Translation is measured in units of 10% of the scene scale, while rotation is measured in degrees.

varies across levels: for low granularity, only a list of nouns is used; for high granularity, all sentence types are employed for a comprehensive textual representation; and for maximum granularity, the noun list and all sentence types are combined to generate the most detailed image descriptions.

Evaluation Metrics. We report Relative Distribution Accuracy (RDA) in Fig. 6 to assess distribution learning performance. Unlike prior work ((Kolmet et al., 2022), (Xia et al., 2024)), in our task, the ambiguous text input and large-scale scene make it challenging to identify all other positive samples. It is defined as the ratio of the accuracy of the predicted distribution (Acc_{Pred}) to the accuracy of a random distribution (Acc_{rand}) as expressed in Equation (5).

$$RDA = \frac{Acc_{Pred}}{Acc_{rand}}, \quad \text{where} \quad Acc = \frac{n_k}{N} \quad (5)$$

Implementation Details. All experiments were conducted using an NVIDIA A6000 GPU. We implemented DDPM with an 8-layer transformer. For pose representation, we used a quaternion vector for rotation and a translation vector in global coordinates. The training was done with a learning rate of 1×10^{-4} and a CosineWarmup scheduler. We used the Adam optimizer and trained for 30k iterations on most datasets, while for Matrix City Street, was 50k iterations.

We set τ_1 as 0.17 and τ_2 as 0.2 in Algorithm 2.

4.2. Experimental Results

Monte Carlo Dropout Baseline. Monte Carlo Dropout (MCDropout) is a practical technique for approximating Bayesian inference in neural networks by applying dropout not only during training but also at inference time. By randomly deactivating a subset of neurons through dropout masks and sampling multiple forward passes, MCDropout generates an empirical distribution of model outputs. In camera relocalization, this method (Kendall & Cipolla, 2016) estimates a distribution over predicted poses, rather than a single deterministic result. By shifting from point estimates to a broader distribution of solutions, MCDropout empowers the relocalization system to make more informed decisions and manage uncertainty in real-world applications, and also make this method a baseline for a distributional estimation of camera poses.

Distribution Learning. We begin by learning position priors for the diffusion model across each large-scale dataset as shown in Tab. 1. Our results demonstrate that our approach outperforms other baselines in terms of RDA, achieving a high concentration of samples near the ground truth pose, with most poses being highly accurate. On smaller datasets, mixed training enhances performance. However, for larger datasets like Matrix City, mixed training leads to worse results, likely due to the increased ambiguity in text descriptions for large-scale scenes.

Additionally, we validated the effectiveness of the Gaussian splatting-based refinement method. By leveraging text CLIP embeddings and rendering image CLIP embeddings to filter and maximize similarity, we achieved significant improvements in distribution performance across most datasets.

Granularity Experiment. We conduct experiments with varying levels of text granularity, categorizing them into (**Low Granularity**, **High Granularity**, and **Max Granularity**). Note we define noun-based expressions as Low Granularity and sentence-based expressions as High Granularity as shown in Section 3. For image inputs, we consider them as Max Granularity. As shown in Tab. 2, our approach consistently outperforms the baseline, and the RDA score increases when more detailed text descriptions are provided, indicating that the estimated poses align more closely with the ground truth. Additionally, incorporating the most detailed image CLIP features yields the highest RDA score, as illustrated in Fig. 4. However, due to overlap and repetition in the city-level images, a substantial portion of the textual descriptions becomes duplicated. This duplication appears to diminish the benefit of mixing textual and image-based features, leading to our mixed approach being outperformed by the baseline (trained exclusively on images). A more detailed discussion of these observations is provided in Ap-

pendix D.

4.3. Ablations & User Studies

Ablation on text granularity. In Fig. 7, we study how varying text granularity in training affects model performance on the small town dataset. Using the template from Section 3.1, we generate descriptions at four noun-based levels (**1 noun**, **3 nouns**, **5 nouns**, **All nouns**) and three sentence-based levels (**Short sentence**, **Middle sentence**, **Long sentence**). We further explore **All sentences** for every sentence length and **All** for every level of detail, ranging from single nouns to full paragraphs. This ablation provides a clear view of how each degree of textual detail influences overall model performance.

Results indicate that at low granularity, the “**All nouns**” setting achieves the highest RDA (7.68), suggesting that incorporating all nouns provides sufficient information for scene understanding in simple contexts. At high granularity, “**All sentences**” outperforms other settings with the highest RDA (27.27), indicating that detailed textual descriptions enhance the model’s ability to capture complex spatial relationships. For max granularity, “**Middle sentence**” achieves the highest RDA (81.44), slightly outperforming “**1 noun**” (81.32), suggesting that moderate-length sentences effectively balance detail and generality. In terms of overall performance, the “**All**” setting provides a balanced approach, showing competitive RDA values across different granularity levels. Additionally, increasing sentence length from “**Short sentence**” to “**Long sentence**” improves RDA under high granularity, demonstrating that longer descriptions capture more scene details. Overall, finer text granularity using sentences performs better than using only nouns, with more detailed textual descriptions leading to improved performance under high granularity.

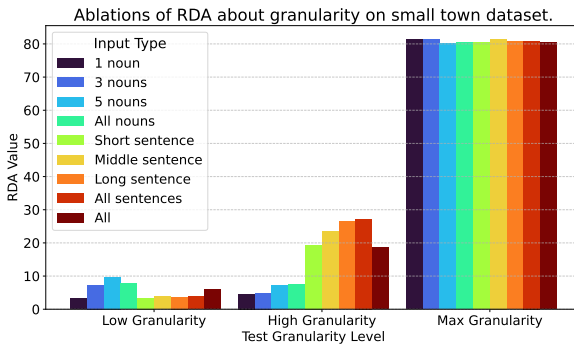


Figure 7. The bar chart compares RDA values across low, high, and maximum granularity levels for different input types for training, including varying numbers of nouns and sentences. The results indicate that increasing granularity and incorporating more descriptive text generally improve RDA performance.

Ablation on swap ratio β . We conducted additional experiments on the swap ratio β to investigate its effect on overall

performance, as presented in Fig. 8. Results show that increasing the swap probability from 0 to 0.7 consistently boosts the RDA score, suggesting that introducing moderate diversity in the training data helps the model capture more robust representations. However, when the swap probability exceeds 0.7, performance begins to degrade slightly, indicating that excessive swapping introduces too much noise. Overall, a moderate swap ratio of around 0.7 appears to offer an optimal balance between enhanced diversity and noise control.

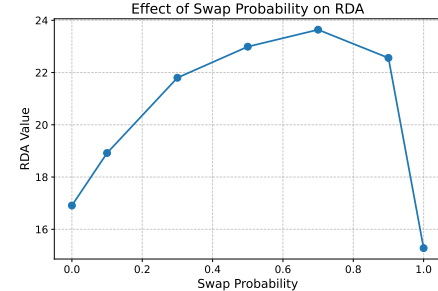


Figure 8. Ablations about swap probability.

User Studies. To validate the effectiveness of our method intuitively, we propose the user studies with question *Which image do you think matches the text description?* (The answer can be multiple selections) as shown in Fig. 5.

Poses	GT	Ours
Match Rate (%)	56.5	50.8

Table 3. User Study

In particular, 10 samples are selected randomly from the output of our method (For each sample,

there are 4 options from our method and 1 ground truth option). Then 30 volunteers are involved to answer this question. Then we compute the average match rate for GT and ours. From the results, in 30% cases the performance of rendered images exceeds that of the ground-truth (GT) images. Overall, our rendered outputs are on par with the GT images, yielding performance comparable to real data. The corresponding results are shown in Tab. 3.

5. Conclusion

We presented a diffusion-based framework for text-based 6DoF localization at the city scale, addressing ambiguity and scalability challenges in large, complex environments. By leveraging 3D Gaussian splatting for efficient pose refinement through text and rendered image similarity optimization, our method achieves superior localization accuracy. Thanks to the Gaussian splatting-based scene representation that allows us to perform the visual reasoning during the refinement step. Applied across diverse large-scale scenes, our approach bridges text and visual understanding, enabling natural human-robot interaction and enhancing multi-modal reasoning in visual environments.

References

Alayrac, J.-B., Donahue, J., Luc, P., Miech, A., Barr, I., Hasson, Y., Lenc, K., Mensch, A., Millican, K., Reynolds, M., et al. Flamingo: a visual language model for few-shot learning. *Advances in neural information processing systems*, 35:23716–23736, 2022.

Amit, T., Nachmani, E., Shaharbany, T., and Wolf, L. Segdiff: Image segmentation with diffusion probabilistic models. *arXiv preprint arXiv:2112.00390*, 2021.

Austin, J., Johnson, D. D., Ho, J., Tarlow, D., and van den Berg, R. Structured denoising diffusion models in discrete state-spaces. In *NeurIPS*, pp. 17981–17993, 2021.

Bai, J., Bai, S., Yang, S., Wang, S., Tan, S., Wang, P., Lin, J., Zhou, C., and Zhou, J. Qwen-vl: A frontier large vision-language model with versatile abilities. *arXiv preprint arXiv:2308.12966*, 2023.

Barron, J. T., Mildenhall, B., Tancik, M., Hedman, P., Martin-Brualla, R., and Srinivasan, P. P. Mip-nerf: A multiscale representation for anti-aliasing neural radiance fields. *ICCV*, 2021.

Barron, J. T., Mildenhall, B., Verbin, D., Srinivasan, P. P., and Hedman, P. Mip-nerf 360: Unbounded anti-aliased neural radiance fields. *CVPR*, 2022.

Brempong, E. A., Kornblith, S., Chen, T., Parmar, N., Minderer, M., and Norouzi, M. Denoising pretraining for semantic segmentation. In *CVPR*, pp. 4175–4186, 2022.

Brown, T., Mann, B., Ryder, N., Subbiah, M., Kaplan, J. D., Dhariwal, P., Neelakantan, A., Shyam, P., Sastry, G., Askell, A., et al. Language models are few-shot learners. *Advances in neural information processing systems*, 33: 1877–1901, 2020.

Chen, K., Zhang, Z., Zeng, W., Zhang, R., Zhu, F., and Zhao, R. Shikra: Unleashing multimodal llm’s referential dialogue magic. *arXiv preprint arXiv:2306.15195*, 2023.

Chowdhery, A., Narang, S., Devlin, J., Bosma, M., Mishra, G., Roberts, A., Barham, P., Chung, H. W., Sutton, C., Gehrmann, S., et al. Palm: Scaling language modeling with pathways. *Journal of Machine Learning Research*, 24(240):1–113, 2023.

Dai, W., Li, J., Li, D., Tiong, A. M. H., Zhao, J., Wang, W., Li, B., Fung, P. N., and Hoi, S. Instructblip: Towards general-purpose vision-language models with instruction tuning. *Advances in Neural Information Processing Systems*, 36, 2024.

Dhariwal, P. and Nichol, A. Diffusion models beat gans on image synthesis. In *NeurIPS*, pp. 8780–8794, 2021.

Ho, J., Jain, A., and Abbeel, P. Denoising diffusion probabilistic models. In *NeurIPS*, pp. 6840–6851, 2020.

Ho, J., Salimans, T., Gritsenko, A., Chan, W., Norouzi, M., and Fleet, D. J. Video diffusion models. *arXiv preprint arXiv:2204.03458*, 2022.

Hoffmann, J., Borgeaud, S., Mensch, A., Buchatskaya, E., Cai, T., Rutherford, E., Casas, D. d. L., Hendricks, L. A., Welbl, J., Clark, A., et al. Training compute-optimal large language models. *arXiv preprint arXiv:2203.15556*, 2022.

Kendall, A. and Cipolla, R. Modelling uncertainty in deep learning for camera relocalization, 2016. URL <https://arxiv.org/abs/1509.05909>.

Kendall, A., Grimes, M., and Cipolla, R. Posenet: A convolutional network for real-time 6-dof camera relocalization. In *Proceedings of the IEEE international conference on computer vision*, pp. 2938–2946, 2015.

Kerbl, B., Kopanas, G., Leimkühler, T., and Drettakis, G. 3d gaussian splatting for real-time radiance field rendering. *ACM Trans. Graph.*, 42(4):139–1, 2023.

Kerbl, B., Meuleman, A., Kopanas, G., Wimmer, M., Lanvin, A., and Drettakis, G. A hierarchical 3d gaussian representation for real-time rendering of very large datasets, 2024. URL <https://arxiv.org/abs/2406.12080>.

Kolmet, M., Zhou, Q., Ošep, A., and Leal-Taixé, L. Text2pos: Text-to-point-cloud cross-modal localization. In *Proceedings of the IEEE/CVF Conference on Computer Vision and Pattern Recognition*, pp. 6687–6696, 2022.

Lai, X., Tian, Z., Chen, Y., Li, Y., Yuan, Y., Liu, S., and Jia, J. Lisa: Reasoning segmentation via large language model. In *Proceedings of the IEEE/CVF Conference on Computer Vision and Pattern Recognition*, pp. 9579–9589, 2024.

Le Scao, T., Fan, A., Akiki, C., Pavlick, E., Ilić, S., Hesslow, D., Castagné, R., Luccioni, A. S., Yvon, F., Gallé, M., et al. Bloom: A 176b-parameter open-access multilingual language model. *arXiv preprint arXiv:2211.05100*, 2023.

Li, B., Zhang, Y., Chen, L., Wang, J., Yang, J., and Liu, Z. Otter: A multi-modal model with in-context instruction tuning, 2023a.

Li, C., Wong, C., Zhang, S., Usuyama, N., Liu, H., Yang, J., Naumann, T., Poon, H., and Gao, J. Llava-med: Training a large language-and-vision assistant for biomedicine in one day. *Advances in Neural Information Processing Systems*, 36, 2024.

Li, J., Li, D., Savarese, S., and Hoi, S. Blip-2: Bootstrapping language-image pre-training with frozen image encoders and large language models. In *International conference on machine learning*, pp. 19730–19742. PMLR, 2023b.

Li, X. L., Thickstun, J., Gulrajani, I., Liang, P., and Hashimoto, T. B. Diffusion-lm improves controllable text generation. *arXiv preprint arXiv:2205.14217*, 2022.

Li, Y., Jiang, L., Xu, L., Xiangli, Y., Wang, Z., Lin, D., and Dai, B. Matrixcity: A large-scale city dataset for city-scale neural rendering and beyond. In *Proceedings of the IEEE/CVF International Conference on Computer Vision*, pp. 3205–3215, 2023c.

Lin, B., Tang, Z., Ye, Y., Cui, J., Zhu, B., Jin, P., Huang, J., Zhang, J., Pang, Y., Ning, M., et al. Moe-llava: Mixture of experts for large vision-language models. *arXiv preprint arXiv:2401.15947*, 2024.

Lin, L., Liu, Y., Hu, Y., Yan, X., Xie, K., and Huang, H. Capturing, reconstructing, and simulating: the urbanscene3d dataset. In *ECCV*, pp. 93–109, 2022.

Liu, C., Zhao, M., Ren, B., Liu, M., Sebe, N., et al. Spatio-temporal graph diffusion for text-driven human motion generation. In *BMVC*, pp. 722–729, 2023a.

Liu, H., Li, C., Wu, Q., and Lee, Y. J. Visual instruction tuning, 2023b.

Liu, H., Li, C., Wu, Q., and Lee, Y. J. Visual instruction tuning, 2023c. URL <https://arxiv.org/abs/2304.08485>.

Liu, H., Li, C., Li, Y., Li, B., Zhang, Y., Shen, S., and Lee, Y. J. Llava-next: Improved reasoning, ocr, and world knowledge, January 2024a. URL <https://llava-vl.github.io/blog/2024-01-30-llava-next/>.

Liu, H., Li, C., Wu, Q., and Lee, Y. J. Visual instruction tuning. *Advances in neural information processing systems*, 36, 2024b.

Liu, Y., Guan, H., Luo, C., Fan, L., Peng, J., and Zhang, Z. Citygaussian: Real-time high-quality large-scale scene rendering with gaussians, 2024c.

Lou, H., Liu, Y., Pan, Y., Geng, Y., Chen, J., Ma, W., Li, C., Wang, L., Feng, H., Shi, L., et al. Robo-gs: A physics consistent spatial-temporal model for robotic arm with hybrid representation. *arXiv preprint arXiv:2408.14873*, 2024.

Lyu, Z., Kong, Z., Xu, X., Pan, L., and Lin, D. A conditional point diffusion-refinement paradigm for 3d point cloud completion. *arXiv preprint arXiv:2112.03530*, 2021.

Ma, Q., Li, Y., Ren, B., Sebe, N., Konukoglu, E., Gevers, T., Van Gool, L., and Paudel, D. P. Shapesplat: A large-scale dataset of gaussian splats and their self-supervised pretraining. In *International Conference on 3D Vision*, 2025.

Mildenhall, B., Srinivasan, P. P., Tancik, M., Barron, J. T., Ramamoorthi, R., and Ng, R. Nerf: Representing scenes as neural radiance fields for view synthesis. *Communications of the ACM*, 65(1):99–106, 2021.

Müller, T., Evans, A., Schied, C., and Keller, A. Instant neural graphics primitives with a multiresolution hash encoding. *ACM Trans. Graph.*, 41(4):102:1–102:15, July 2022. doi: 10.1145/3528223.3530127. URL <https://doi.org/10.1145/3528223.3530127>.

Peng, Z., Wang, W., Dong, L., Hao, Y., Huang, S., Ma, S., and Wei, F. Kosmos-2: Grounding multimodal large language models to the world. *arXiv preprint arXiv:2306.14824*, 2023.

Popov, V., Vovk, I., Gogoryan, V., Sadekova, T., and Kudinov, M. Grad-tts: A diffusion probabilistic model for text-to-speech. In *ICML*, pp. 8599–8608, 2021.

Radford, A., Kim, J. W., Hallacy, C., Ramesh, A., Goh, G., Agarwal, S., Sastry, G., Askell, A., Mishkin, P., Clark, J., Krueger, G., and Sutskever, I. Learning transferable visual models from natural language supervision, 2021. URL <https://arxiv.org/abs/2103.00020>.

Ramesh, A., Pavlov, M., Goh, G., Gray, S., Voss, C., Radford, A., Chen, M., and Sutskever, I. Zero-shot text-to-image generation, 2021. URL <https://arxiv.org/abs/2102.12092>.

Ren, B., Liu, M., Ding, R., and Liu, H. A survey on 3d skeleton-based action recognition using learning method. *Cyborg and Bionic Systems*, 5:0100, 2024.

Schönberger, J. L. and Frahm, J.-M. Structure-from-Motion Revisited. In *Conference on Computer Vision and Pattern Recognition (CVPR)*, 2016.

Singer, U., Polyak, A., Hayes, T., Yin, X., An, J., Zhang, S., Hu, Q., Yang, H., Ashual, O., Gafni, O., et al. Make-a-video: Text-to-video generation without text-video data. *arXiv preprint arXiv:2209.14792*, 2022.

Sohl-Dickstein, J., Weiss, E., Maheswaranathan, N., and Ganguli, S. Deep unsupervised learning using nonequilibrium thermodynamics. In *ICML*, pp. 2256–2265, 2015.

Song, J., Meng, C., and Ermon, S. Denoising diffusion implicit models. *arXiv preprint arXiv:2010.02502*, 2020.

Sun, Y., Wang, X., Zhang, Y., Zhang, J., Jiang, C., Guo, Y., and Wang, F. icomma: Inverting 3d gaussians splatting for camera pose estimation via comparing and matching. *arXiv preprint arXiv:2312.09031*, 2023.

Tancik, M., Casser, V., Yan, X., Pradhan, S., Mildenhall, B., Srinivasan, P. P., Barron, J. T., and Kretzschmar, H. Block-nerf: Scalable large scene neural view synthesis. In *Proceedings of the IEEE/CVF Conference on Computer Vision and Pattern Recognition*, pp. 8248–8258, 2022.

Touvron, H., Lavril, T., Izacard, G., Martinet, X., Lachaux, M.-A., Lacroix, T., Rozière, B., Goyal, N., Hambro, E., Azhar, F., et al. Llama: Open and efficient foundation language models. *arXiv preprint arXiv:2302.13971*, 2023.

Turki, H., Ramanan, D., and Satyanarayanan, M. Mega-nerf: Scalable construction of large-scale nerfs for virtual fly-throughs. In *Proceedings of the IEEE/CVF Conference on Computer Vision and Pattern Recognition*, pp. 12922–12931, 2022.

Wang, G., Fan, H., and Kankanhalli, M. Text to point cloud localization with relation-enhanced transformer. In *Proceedings of the AAAI Conference on Artificial Intelligence*, volume 37, pp. 2501–2509, 2023a.

Wang, J., Rupprecht, C., and Novotny, D. Posediffusion: Solving pose estimation via diffusion-aided bundle adjustment. In *Proceedings of the IEEE/CVF International Conference on Computer Vision*, pp. 9773–9783, 2023b.

Wang, W., Chen, Z., Chen, X., Wu, J., Zhu, X., Zeng, G., Luo, P., Lu, T., Zhou, J., Qiao, Y., et al. Visionllm: Large language model is also an open-ended decoder for vision-centric tasks. *NeurIPS*, 2023c.

Wang, Y., Yu, J., and Zhang, J. Zero-shot image restoration using denoising diffusion null-space model. In *ICLR*, 2022.

Wu, Z., Liu, T., Luo, L., Zhong, Z., Chen, J., Xiao, H., Hou, C., Lou, H., Chen, Y., Yang, R., et al. Mars: An instance-aware, modular and realistic simulator for autonomous driving. In *CAAI International Conference on Artificial Intelligence*, pp. 3–15. Springer, 2023.

Xia, Y., Shi, L., Ding, Z., Henriques, J. F., and Cremers, D. Text2loc: 3d point cloud localization from natural language. In *Proceedings of the IEEE/CVF Conference on Computer Vision and Pattern Recognition*, pp. 14958–14967, 2024.

Yang, R., Zhu, Z., Jiang, Z., Ye, B., Chen, X., Zhang, Y., Chen, Y., Zhao, J., and Zhao, H. Spectrally pruned gaussian fields with neural compensation. *arXiv preprint arXiv:2405.00676*, 2024.

Ye, Q., Xu, H., Xu, G., Ye, J., Yan, M., Zhou, Y., Wang, J., Hu, A., Shi, P., Shi, Y., et al. mplug-owl: Modularization empowers large language models with multimodality. *arXiv preprint arXiv:2304.14178*, 2023.

Yen-Chen, L., Florence, P., Barron, J. T., Rodriguez, A., Isola, P., and Lin, T.-Y. inerf: Inverting neural radiance fields for pose estimation. In *2021 IEEE/RSJ International Conference on Intelligent Robots and Systems (IROS)*, pp. 1323–1330. IEEE, 2021.

Yin, S., Fu, C., Zhao, S., Li, K., Sun, X., Xu, T., and Chen, E. A survey on multimodal large language models. *arXiv preprint arXiv:2306.13549*, 2023.

You, H., Zhang, H., Gan, Z., Du, X., Zhang, B., Wang, Z., Cao, L., Chang, S.-F., and Yang, Y. Ferret: Refer and ground anything anywhere at any granularity. *arXiv preprint arXiv:2310.07704*, 2023.

Zhang, A., Zhao, L., Xie, C.-W., Zheng, Y., Ji, W., and Chua, T.-S. Next-chat: An lmm for chat, detection and segmentation. *arXiv preprint arXiv:2311.04498*, 2023.

Zhao, M., Liu, M., Ren, B., Dai, S., and Sebe, N. Denoising diffusion probabilistic models for action-conditioned 3d motion generation. In *ICASSP 2024-2024 IEEE International Conference on Acoustics, Speech and Signal Processing (ICASSP)*, pp. 4225–4229. IEEE, 2024.

Zheng, Y., Chen, X., Zheng, Y., Gu, S., Yang, R., Jin, B., Li, P., Zhong, C., Wang, Z., Liu, L., et al. Gaussiangrasper: 3d language gaussian splatting for open-vocabulary robotic grasping. *arXiv preprint arXiv:2403.09637*, 2024.

Zhu, D., Chen, J., Shen, X., Li, X., and Elhoseiny, M. Minigpt-4: Enhancing vision-language understanding with advanced large language models. *arXiv preprint arXiv:2304.10592*, 2023a.

Zhu, D., Chen, J., Shen, X., Li, X., and Elhoseiny, M. Minigpt-4: Enhancing vision-language understanding with advanced large language models. *arXiv preprint arXiv:2304.10592*, 2023b.

In this appendix, we provide additional details to enhance the clarity and comprehensiveness of our work. First, we briefly illustrate two important base techniques, *i.e.*, Diffusion model and Gaussian Splatting in Appendix A. Next, the experimental setups are detailed in Appendix B, followed by an in-depth analysis of the ablation experiments in Appendix C, which demonstrate the effectiveness of our approach. Finally, we discuss further implications and insights in Appendix D and conclude with an exploration of the broader impact of our work in Appendix E.

A. Preliminaries

Diffusion Models. Diffusion models (Ho et al., 2020; Sohl-Dickstein et al., 2015) are a class of likelihood-based generative models that approximate complex data distributions by inverting a diffusion process from data to a simple distribution via noising and denoising. The noising process transforms data samples x into noise over a sequence of $T \in \mathbb{N}$ steps. The model is trained to learn the denoising process.

A Denoising Diffusion Probabilistic Model (DDPM) specifies Gaussian noising. For a variance schedule β_1, \dots, β_T across T steps, the noising transitions are defined as follows:

$$q(x_t | x_{t-1}) = \mathcal{N}(x_t; \sqrt{1 - \beta_t}x_{t-1}, \beta_t \mathbb{I}), \quad (6)$$

where \mathbb{I} is the identity matrix. This schedule ensures x_T approaches an isotropic Gaussian, *i.e.*, $q(x_T) \approx \mathcal{N}(\mathbf{0}, \mathbb{I})$. Setting $\alpha_t = 1 - \beta_t$ and $\bar{\alpha}_t = \prod_{i=1}^t \alpha_i$ yields a closed-form solution for directly sampling x_t given a data point x_0 :

$$x_t \sim q(x_t | x_0) = \mathcal{N}(x_t; \sqrt{\bar{\alpha}_t}x_0, (1 - \bar{\alpha}_t)\mathbb{I}). \quad (7)$$

For sufficiently small β_t , the reverse $p_\theta(x_{t-1} | x_t)$ is Gaussian. Thus, we approximate it with model \mathcal{F}_θ :

$$p_\theta(x_{t-1} | x_t) = \mathcal{N}(x_{t-1}; \sqrt{\alpha_t}\mathcal{F}_\theta(x_t, t), (1 - \alpha_t)\mathbb{I}). \quad (8)$$

3D Gaussian Splatting. 3DGS represents scene space with Gaussian primitives $\{Y_i\}_{i=1}^N$, stacking these as follows:

$$Y = [C, O, S, R, SH] \in \mathbb{R}^{N \times 59}, \quad (9)$$

where $C \in \mathbb{R}^{N \times 3}$ denotes the centroid, $O \in \mathbb{R}^{N \times 1}$ the opacity, $S \in \mathbb{R}^{N \times 3}$ the scale, $R \in \mathbb{R}^{N \times 4}$ the quaternion rotation vector, and $SH \in \mathbb{R}^{N \times 48}$ the spherical harmonics. These are collectively termed Gaussian parameters. Each Gaussian softly represents a spatial area with opacity. A point q in the scene space is influenced by a Gaussian Y_i according to the Gaussian distribution, weighted by opacity:

$$h_i(q) = O_i \exp \left(-\frac{1}{2}(q - C_i)^T \Sigma_i^{-1} (q - C_i) \right), \quad (10)$$

where covariance Σ_i is formulated as $\Sigma_i = R_i S_i S_i^T R_i^T$.

Projected onto a 2D image plane, each Gaussian's influence, h , contributes to a pixel's color through an alpha-blending equation over the set \mathcal{G} of influencing Gaussians:

$$c_{\text{pixel}} = \sum_{i \in \mathcal{G}} c_i h_i^{2D} \prod_{j=1}^{i-1} (1 - h_j^{2D}). \quad (11)$$

Through differentiable rasterization, rendering losses are back-propagated to update the Gaussian parameters. In this manner, we represent images rendered from pose P given by $I = \mathcal{G}(P)$.

B. Experimental Setups

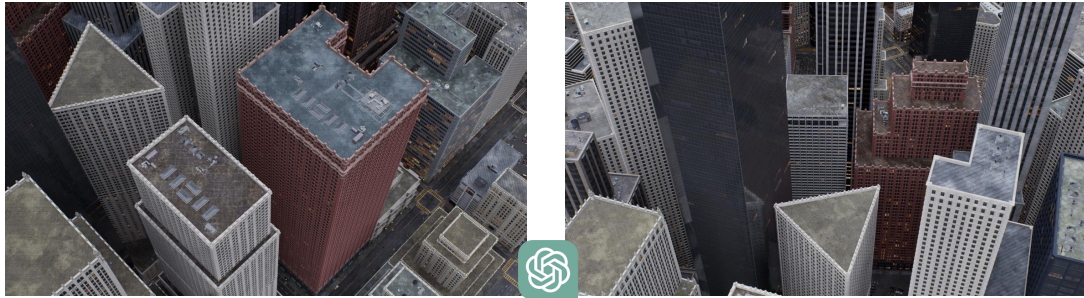
Gaussian Training. To process large-scale scenes, we utilize H3DGS (Kerbl et al., 2024) for Gaussian training. Chunk sizes are set to 100×100 for street views and 200×200 for aerial views. The datasets are partitioned into the following chunks: 4 for the small town dataset, 2 for the SciArt dataset, 4 for the residence dataset, 66 for the Matrix City aerial dataset, and 203 for the Matrix City small dataset. Each chunk is trained for 60,000 iterations. Subsequently, chunks are merged following hierarchy optimization; however, for the Matrix City dataset, memory constraints as shown in Fig.2 of our main manuscript prevent merging all chunks. Instead, only adjacent chunks are merged with overlap. For each dataset, we first use the training views from regarding dataset to construct the Gaussian splats. Subsequently, we randomly select 10% of the poses as the validation set, while the remaining 90% are used to train the diffusion model.

Diffusion Model Training. In addition to the details mentioned in our main manuscript, for each batch, we randomly select 90 different timesteps out of a total of 100. We optimize the noise prediction step-by-step with a dropout rate of 0.1. The beta scheduler follows a linear progression from 1×10^{-4} to 0.1. For optimization, we use an L_1 loss function for both translation and rotation quaternions. For the CLIP model, we use the pretrained laion2bs34b-b88k. For LLava, we utilize the lmms-lab/llama3-llava-next-8b model.

Details of Gaussian based refinement. To identify the pose that best matches the text embedding at the feature level from the many possible outputs of a diffusion model, we propose the Gaussian Refinement Algorithm (Algorithm 2). This algorithm iteratively refines an initial coarse pose by aligning its rendered view with the corresponding textual description in the embedding space, leveraging city-scale Gaussian models and the expressiveness of CLIP embeddings to achieve robust text-to-pose refinement.

The refinement process begins with a coarse camera pose, which is used to render a synthetic view based on the Gaus-

Llava: The image shows a cityscape with tall buildings. The buildings are of various designs and heights. The photo is taken from an aerial perspective.



This image shows a dense cityscape with a **reddish-brown building** standing out among gray and white skyscrapers, including a **triangular-roofed** structure in the foreground. rooftops feature detailed urban infrastructure like vents and HVAC units. The **faint streets** below add depth to the scene.

This view highlights a **towering black skyscraper** **surrounded by** reddish-brown and gray buildings of varied styles. The **triangular building** reappears, contrasting with the square and rectangular forms around it. Detailed rooftops and visible streets emphasize the urban density.

Figure 9. Limitations on generated text for large scale scene: We used the Llava model for image captioning at different granularities, but we found that for larger and more complex scenes, the text generated by Llava fails to extract more effective information. For example, as shown in the image above, for two pictures with numerous city buildings, Llava fails to generate distinct text prompts. In contrast, ChatGPT provides very detailed information that is helpful for localization.

sian model and pipeline parameters. During refinement, we follow the steps outlined in ICOMA, rendering images at a resolution of 224×224 while maintaining the same field of view (FoV). For images with differing aspect ratios, the shorter side is resized to 224 pixels, and the longer side is cropped to match the aspect ratio. Since the rasterization process only allows optimization of one image at a time, optimizing across all poses in the test set would be computationally prohibitive. Thus, refinement is conducted on a randomly selected 10% subset of the test set. In each refinement iteration, the rendered view is normalized and encoded using a CLIP Image Encoder, generating an embedding that is compared to the text embedding from a CLIP Text Encoder. A similarity score is computed between the two embeddings, and the loss is formulated as the negative of this similarity. Using gradient-based optimization, the coarse pose is iteratively updated to maximize the feature-level alignment with the text embedding. To ensure robustness, the algorithm incorporates rejection mechanisms, discarding poses that fail to meet minimum similarity thresholds. By combining Gaussian models with CLIP embeddings and adhering to computationally efficient refinement steps, the Algorithm 2 effectively bridges the gap between text descriptions and 6DoF camera poses, delivering accurate localization results even in large-scale 3D environments.

C. More Visual Results

Qualitative results of granularity. We conducted experiments to evaluate the impact of text granularity across var-

ious datasets, and the results, illustrated in the Fig. 11 - 14, are consistent performs well. A pattern emerges across all datasets: as the text input becomes more detailed, the pose distribution transitions from a high-variance spread to a narrower, more precise distribution. In parallel, the estimated camera poses increasingly align with the given text input. Notably, when the most fine-grained input, such as an image, is used, our method achieves pose estimations that are the closest to the actual input pose.

Qualitative Results of User Study. We present further qualitative results demonstrating how well the rendered images match the ground-truth images in response to various text descriptions, as depicted in Fig. 14. For instance, in image (a), the presence of cars parked on both sides of the street closely matches the described scenario, showcasing the effectiveness of our pose estimation technique. Image (d) particularly highlights the model's capability to discern unique urban features, such as specific building types and road layouts, leading to precise pose estimations.

In images (b) and (c), the alignment of estimated camera poses with more generalized urban scenes shows the robustness of our approach across different settings. For example, in image (b), the estimation aligns well with a typical street scene, demonstrating the model's ability to contextualize and accurately generate relevant poses.

Additionally, image (e) shows an aerial view of city parks juxtaposed against dense urban structures, a challenging scene that tests the limits of our model's contextual understanding. Despite this complexity, the model manages

to provide a plausible estimate that aligns reasonably well with the text description. These examples underscore the potential of our method in practical applications, allowing for accurate and context-aware pose estimations based on varied textual inputs. There are more qualitative results in Fig. 14.

D. Discussion and Limitations

To the best of our knowledge, our work is the first to use a diffusion model based on text to estimate pose distributions. Compared to the baseline, our method effectively identifies scenes that match the text description. Additionally, the Gaussian refinement helps us filter out poor samples and further optimize the pose estimation. Our approach also supports multimodal image inputs. In our experiments, we utilized the Llava model for image captioning at varying granularities. While the model performed well in many cases, we identified a significant limitation when applied to larger and more complex scenes. Specifically, Llava’s generated captions were unable to extract and convey sufficiently detailed information necessary for effective scene understanding, particularly in urban environments with dense structures as shown in Fig. 9. Given these observations, we recognize the need for more powerful Visual Language Models (VLMs) that can generate richer and more accurate captions, especially for complex and large-scale scenes. As part of our future work, we plan to explore and incorporate more advanced VLMs to improve the quality and granularity of the text descriptions generated, which will ultimately enhance performance in tasks such as scene understanding, localization, and cross-modal retrieval.

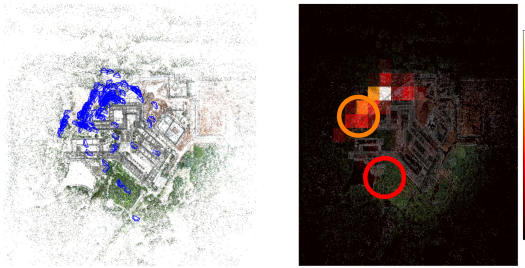
E. Impact Statement

The proposed framework for text-based 6DoF camera localization introduces significant advancements in multi-modal reasoning, with potential impacts across various domains. By enabling precise localization based on ambiguous text descriptions, this method could transform applications such as autonomous navigation, urban planning, and augmented reality. For instance, in smart cities, this framework could aid in mapping and localizing critical infrastructure or guiding autonomous vehicles using natural language instructions. Moreover, the integration of text and visual understanding enhances human-robot interaction, making it easier for non-experts to communicate with AI systems in large-scale, complex environments. The ability to perform visual reasoning with 3D Gaussian splatting also sets the stage for more efficient and scalable representations of urban and virtual scenes, benefiting areas like gaming, simulation, and virtual tourism. However, the broad applicability of this technology may also raise ethical concerns, including potential misuse of surveillance or privacy violations. Ensuring the responsi-

ble deployment of such systems is essential to mitigate these risks. Overall, this work represents a step forward in bridging natural language understanding with spatial reasoning, paving the way for innovative multi-modal AI applications.

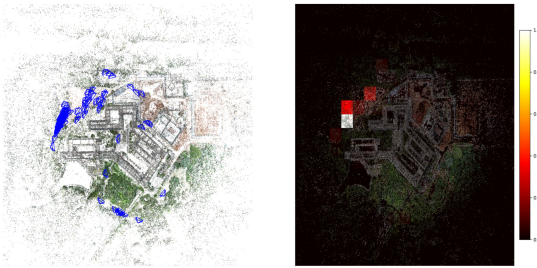


GT Pose and Image

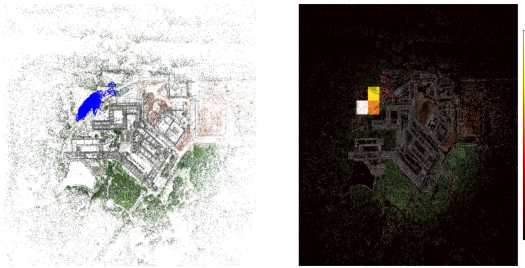


This image shows apartment building.

Estimated Pose and Render Image



This image shows a large building with many windows and a parking lot in front of it..



The image shows a multi-story residential building with a parking lot in front. There are several cars parked in the lot. The building has a mix of red and white exterior walls.

< Image CLIP Feature; >

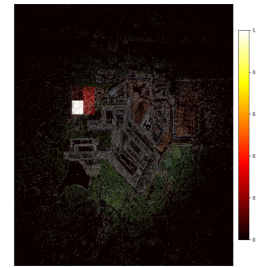
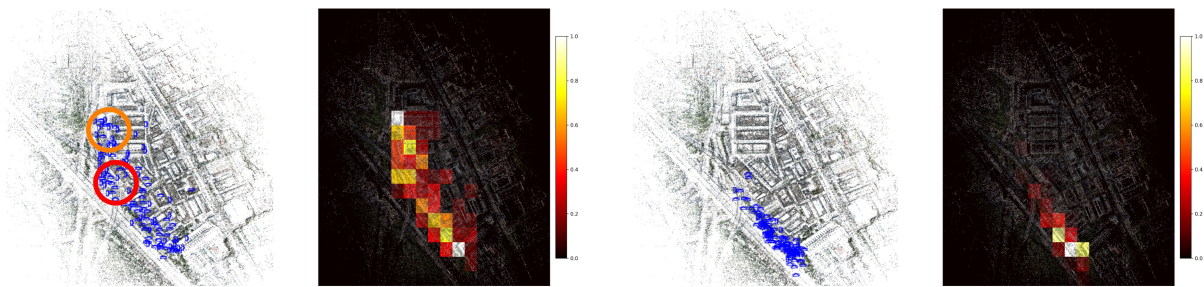


Figure 10. Qualitative Results on the SciArt Dataset: Similarly, we use the [green camera](#) to indicate the camera pose used to generate the prompt, while high-density estimations are shown in [orange camera](#) and [red camera](#). Providing more detailed text conditions results in a narrower distribution of estimated camera poses.



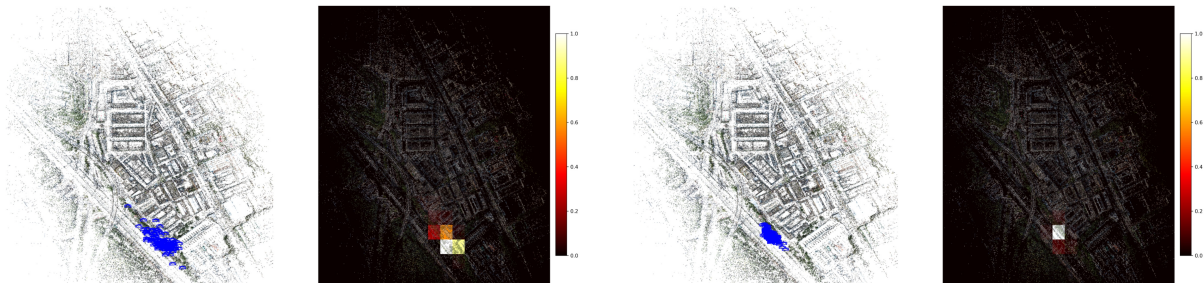
GT Pose and Image

Estimated Pose and Render Image



This image shows highway.

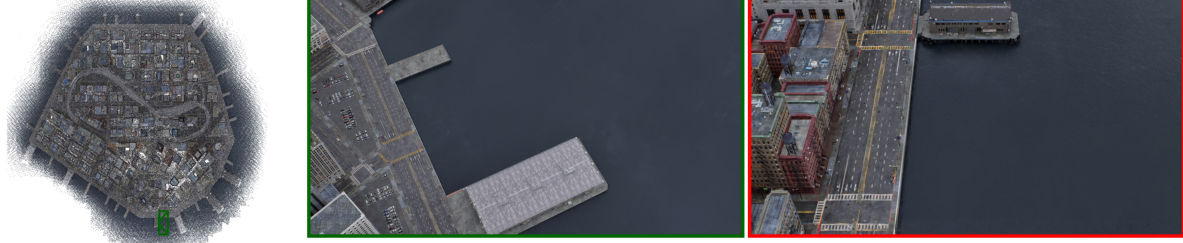
A highway with cars driving on it, with trees on both sides.



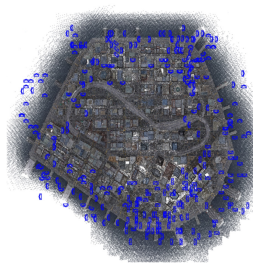
The image shows a highway with multiple lanes, trees on both sides, and a few vehicles.
 The highway is elevated above the surrounding landscape, and the shadow indicate a clear sky

< Image CLIP Feature; >

Figure 11. Qualitative Results on the Residence Dataset: The results demonstrate excellent localization potential. The dataset primarily features a residential area with a highway passing through the left section. When using a general prompt like "The image shows a highway," the estimated camera positions are distributed along the entire highway, successfully aligning with the text prompt. As more detailed information is provided, the estimated positions gradually narrow down and converge closer to the specific locations depicted in the images.



GT Pose and Image



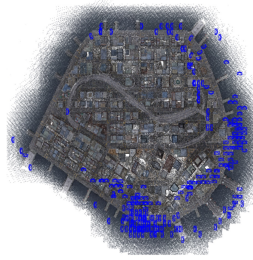
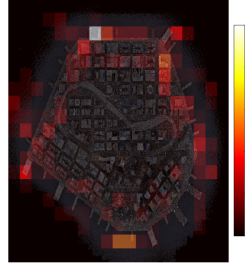
This image shows dock.



Estimated Pose and Render Image



The image shows a body of water with a pier extending into it.



The image shows an aerial view of a body of water with a pier extending into it. There is a parking lot on the left side of the image. The water appears calm.



< Image CLIP Feature; >



Figure 12. Qualitative Results on the Matrix City Aerial Dataset: We observe that our method also performs exceptionally well on large-scale scene datasets. For instance, the [green camera](#) highlights areas such as a dock and a parking lot. When using simpler or moderately detailed descriptions, the heatmap shows that the estimated poses are distributed across many similar scenes within the city that match the description. However, when the text input includes more specific details, such as mentioning the parking lot, the pose distribution suddenly narrows. The [red renderings](#) show areas without parking lots, where no poses are present in the estimated distribution. Finally, when using the given image's CLIP features, we achieve the most accurate pose estimation.

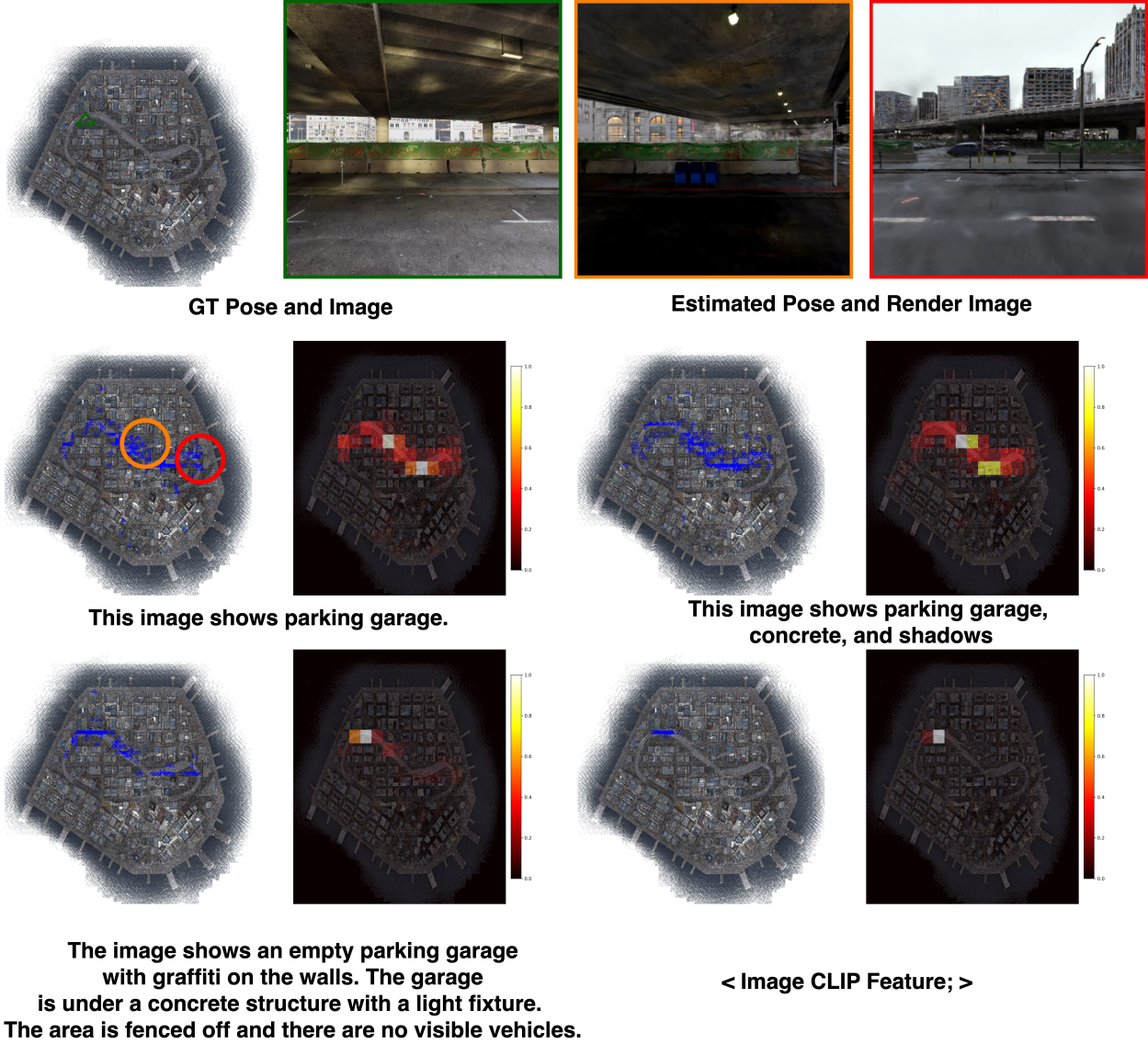


Figure 13. Qualitative Results on the Matrix City Street Dataset: On the urban street dataset, most street data is highly similar, with numerous overlapping text inputs. To address this, we used a more distinctive scenarioa garage under an overpass—as the image input. The results show that when we provide a coarse-grained input like "garage," our method generates poses near all potential parking locations, including not only under the overpass but also next to open-air street garages, as indicated by the **red renderings**. We also observe that as the input text becomes more specific, incorporating details like "shadow," "concrete," and "fence off," the distribution variance decreases, and the estimated poses converge closer to the input pose.

User Study

*Example Question: Which image do you think match with the text description?
(You can select multiple items that match)*



a) A street with cars parked on both sides



b) A street scene with parked cars and a building in the background.



c) A view of a highway with cars and a bridge over it.



d) The image shows an aerial view of a city with various buildings, roads, and parking lots. There are also some green spaces visible.



e) A view of a city from an aerial perspective



f) The image shows an aerial view of a city with various buildings, some of which are under construction. There are trees and roads visible, indicating a mix of urban and green spaces. The architecture suggests a modern cityscape.



g) This image shows parking garage



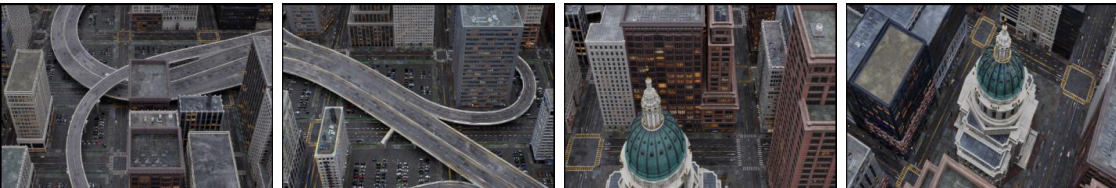
h) The image shows a construction site with a large building under construction. There is a dirt road leading to the site, and construction materials are visible. The surrounding area includes trees and a building that appears to be undergoing renovation.



i) This image shows bank



j) The image shows a bus stop with a shelter and a street sign. There is a large building with reflective glass windows in the background. The street has a number painted on it, indicating a specific location



k) This image shows overpass



l) The image shows a bird's eye view of a cityscape with a prominent dome building in the foreground. The city has a grid-like street pattern and is composed of various buildings of different heights and designs. The architecture suggests a modern urban environment.

Figure 14. Qualitative results of the proposed method: Training images are shown on the left, with the rendered images on the right.